Front. Earth Sci. 2024, 18(2): 412–421
https://doi.org/10.1007/s11707-022-1040-z

RESEARCH ARTICLE

Flow resistance in the channel-bar landscape of large alluvial rivers

Yong HU[1], Congcong LIU[2,3,4,5], Jinyun DENG (✉)[1], Wei ZHANG[1], Yitian LI[1]

1 State Key Laboratory of Water Resources and Hydropower Engineering Science, Wuhan University, Wuhan 430072, China
2 CCCC Second Harbor Engineering Company Ltd, Wuhan 430040, China
3 Key Laboratory of Large-span Bridge Construction Technology, Wuhan 430040, China
4 Research and Development Center of Transport Industry of Intelligent Manufacturing Technologies of Transport Infrastructure, Wuhan 430040, China
5 CCCC Highway Bridge National Engineering Research Centre Co. Ltd, Wuhan 430040, China

Abstract Accurate approaches for estimating flow resistance in large alluvial rivers are fundamental for simulating discharge, sediment transport, and flood routing. However, methods for estimating riverbed resistance and additional resistance in the channel-bar landscapes remain poorly investigated. In this study, we used *in situ* river bathymetry, sediment, and hydraulic data from the Shashi Reach in the Yangtze River to develop a semi-empirical approach for calculating flow resistance. Our method quantitatively separates flow resistance into riverbed resistance and additional resistance and shows high accuracy in terms of deviation ratio (~20%), root-mean-square error (~0.008), and geometric standard deviation (~3). Additional resistance plays a dominant role under low-flow conditions but a secondary role under high flows, primarily due to the reduction in momentum exchange in channel-bar regions as discharge increases. Riverbed resistance first decreases and then increases, which might be attributed to bedform changes in the lower and transitional flow regimes as flow velocity increases. Overall, our findings further the understanding of dynamic changes in flow resistance in the channel-bar landscapes of large river systems and have important implications for riverine ecology and flood management.

Keywords flow resistance, channel-bar landscape, interaction region, large river, bedform

1 Introduction

Scientific investigations of the controls on river depth and velocity began in the 1700s and there is now a large and continually growing body of literature on the topic, including several reviews of flow resistance (Ferguson, 2013; Powell, 2014; Dai, 2021). Almost all the existing literature refers to the main channels of natural or engineered alluvial or bedrock rivers (Church and Ferguson, 2015; Ferguson et al., 2017; Mei et al., 2018). In contrast, very little is known about the bulk hydraulics of channel-bar interaction regions in large rivers, particularly their flow resistance behaviors (Mohanta et al., 2021; Ferguson et al., 2022).

Channel-bar interaction regions, which are the transition areas between main channels and high bars, occur in most large rivers worldwide and display complex flow movement (Dai et al., 2018; Mohanta et al., 2021). Previous experimental studies have observed lateral momentum transfer in these regions due to the channel-bar flow velocity difference (van Prooijen et al., 2005). In turn, the complicated flow and sediment regimes in interaction regions can influence the accuracy of discharge, sediment transport, and flood routing simulations (Chen et al., 2019a; Ferguson, 2021). Nevertheless, recent studies on flow resistance prediction have focused on laboratory-based methods (Knight et al., 2018; Chandra, 2019), and changes in individual resistance components under variable hydraulic geometry conditions are very rarely reported (Ferguson et al., 2019).

Currently, large rivers are subject to ongoing environmental change, including fluctuations in climate (Dai, 2021; Li et al., 2021) and human activity (Tellman et al., 2021; Lou et al., 2022; Zhou et al., 2022), and the responses of flow resistance to these changes have been widely noted (Church and Ferguson, 2015). However, flow and sediment parameters in channel-bar interaction

Received April 19, 2022; accepted August 31, 2022

E-mail: dengjinyun@whu.edu.cn

regions remain poorly documented because of the practical challenges of measurement, especially at high flows (Chen et al., 2016, 2019b). Indeed, many previous studies have ignored lateral momentum transfer when estimating flow velocities in large rivers with channel-bar landscapes (Huthoff et al., 2008; Proust et al., 2009). Furthermore, commercial modeling tools, such as SOBEK, MIKE, and HEC-RAS, assume that no lateral momentum transfer occurs (Huthoff et al., 2008). Alternative approaches include the following: 1) continuing to ignore lateral momentum transfer while shifting the position and shape of interfaces (Patra and Kar, 2000; Cassells et al., 2001); 2) describing lateral momentum transfer by introducing the apparent shear stress (Christodoulou, 1992; Bousmar and Zech, 1999; Moreta and Martin-Vide, 2010; Chen et al., 2016; Chandra, 2019); and 3) resorting to a continuum model that resolves flow velocity as a function of the cross-channel coordinate (Shiono and Knight, 1991; van Prooijen et al., 2005). However, these methods are mainly based on laboratory experiments, and their applicability to large rivers is questionable (Chen et al., 2019a). Moreover, there is still a lack of attention on quantitatively assessing the relative contributions of different sources to flow resistance as well as evaluating the impacts of hydraulic geometry and flow regimes on flow resistance (Chandra, 2019).

In situ bathymetry, flow, and sedimentary data sets from 2004 to 2018 at the Shashi Reach, a representative channel-bar-type reach in the Yangtze River (Fig. 1), provide a rare opportunity to quantify the flow resistance in the interaction regions of large rivers. The reliability and robustness of these data obtained under low- and high-flow conditions offer advantages over empirical or physical-based models, which are commonly associated with inherent uncertainties (Paarlberg et al., 2009; Ferguson et al., 2022). In particular, we were able to decompose total resistance into its component parts and evaluate their variations under different hydraulic geometry conditions. The specific objectives of this study were to 1) develop a semi-empirical approach for flow resistance calculation, 2) quantify the contributions of each resistance component to total resistance, and 3) clarify the change law of flow resistance in response to hydraulic geometry in the channel-bar-type landscapes of large alluvial rivers. The study findings enhance our understanding of the dynamic changes in flow resistance in channel-bar landscapes in large river systems and have important implications for riverine ecology and flood management.

2 Data and methods

2.1 Study area

The Yangtze River is 6300 km long and is usually divided into three parts—the upper Yangtze (source to Yichang), middle Yangtze (Yichang to Hukou), and lower Yangtze (Hukou to Datong) (Li et al., 2019; He et al., 2022). The middle Yangtze River (MYR) is characterized by a subtropical monsoon climate with an average annual temperature ranging from 15°C to 19°C and an average annual precipitation of 1000 mm (Yang et al., 2015). The Shashi Reach is located 170 km downstream of the Three Gorges Dam (TGD) in the

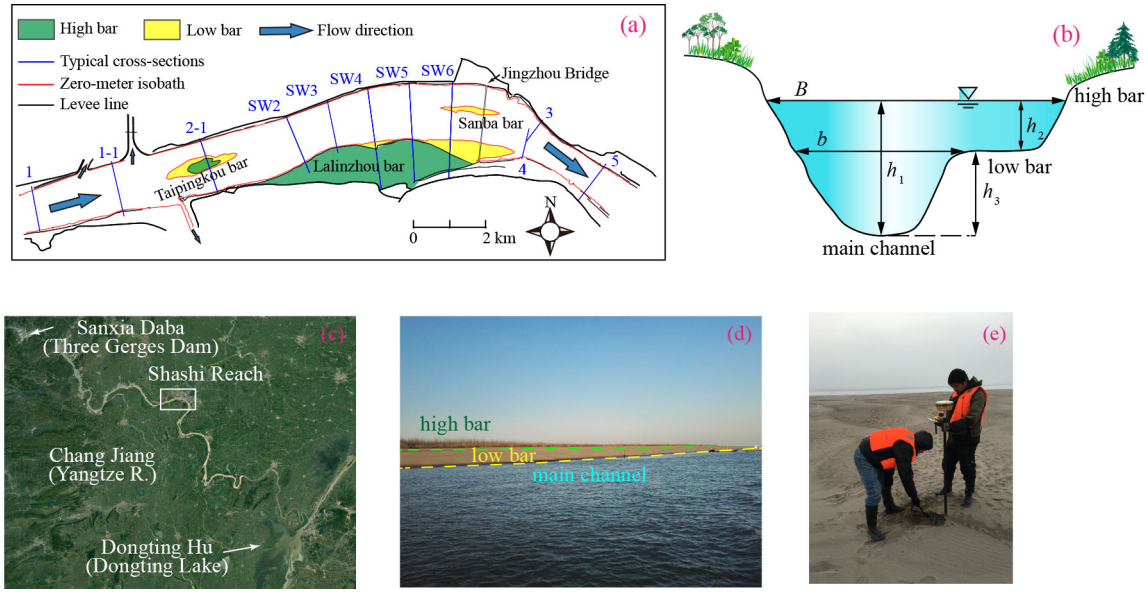

Fig. 1 Sketch map and photos of the study area: (a) the Shashi Reach; (b) a typical cross-section profile; (c) the Change Jiang Basin; (d) photo showing the channel, low bar, and high bar areas (taken by Wei Liu in December 2015); and (e) photo showing the sampling of the low bar (taken by Chi Fu in December 2015).

MYR (Fig. 1). The Shashi Reach is a part of the Upper Jingjiang Reach, which is one of the most dynamic reaches along the MYR (Xia et al., 2016).

The Shashi Reach displays a meandering and bar-braided channel pattern characteristic of the morphology of meandering channels (Hooke and Yorke, 2011; Wang et al., 2018). The sand-bed channels in the MYR begin in the Shashi Reach, covering approximately 18 km from Chenjiawan to Yuheping. Therefore, grain size and hydraulic parameters in this reach are sensitive to the operation of the Three Gorges Dam, and hence it is convenient to evaluate flow resistance response with in situ data. Additionally, it is a representative reach in the MYR with a channel-bar landscape. Several bars are located in this reach: the Taipingkou mid-channel bar upstream of Jingzhou Bridge, the Lalinzhou point bar on the convex side of the bend, and the Sanba mid-channel bar beneath the bridge. Based on the bathymetric elevation in the Shashi Reach, a high bar with an elevation greater than 38 m, and a channel-bar interaction region with an elevation between 32 and 38 m, were selected for this study (Fig. 1).

2.2 Data collection

Hydrological, topographical, and riverbed sediment grain-size data for the Shashi Reach for August 2003, November 2003, August 2010, November 2010, August 2015, December 2015, March 2018, and August 2018 were obtained from the Changjiang Water Resources Commission. Data were processed according to a set of strict survey protocols issued by the Ministry of Water Resources (i.e., "Code for Liquid Flow Measurement in Open Channels" (GB-50179-2015)), ensuring an accuracy of > 95%. The topographical and sediment data were collected from the Changjiang Waterway Bureau (CWB), and the bathymetric survey followed the survey protocols of the "Specifications for Port and Waterway Engineering Survey" (JTS/T231-2021), which ensures a horizontal error of ⩽ 1 m and vertical error of ⩽ 0.1 m (Li et al., 2019). In total, approximately 5500 elevation points were obtained in the Shashi Reach (18 km in length and 1.5 km in width) with a spatial resolution of approximately 100 m × 40 m (river flow direction × river width direction), which is comparable to that of other large rivers including, the Rhine in Germany (Arnaud et al., 2019) and the Missouri in the USA (Skalak et al., 2013).

The hydraulic, topographic, and granulometric parameters of the channel-bar interaction regions of the Shashi Reach were divided into the eight groups summarized in Table 1. Each set of data covered discharge (Q, m^3/s), total channel width (B, m), main channel width (b, m), total water depth (h_1, m), channel-bar interaction region water depth (h_2, m), main channel water depth ($h_3 = h_1 - h_2$, m), average flow velocity (U, m/s), median grain size of bed material (D_{50}, mm), energy slope (J, -), and Froude number (Fr, -). Based on long-term statistics, the discharge of the Shashi Reach is approximately 10000 m^3/s (low-flow channel) during the dry season and 35000 m^3/s (high-flow channel) during the flood season.

2.3 Estimating flow resistance in the channel-bar interaction region

The flow resistance in the channel-bar interaction region mainly consists of form resistance (Ferguson et al., 2019), grain resistance (Powell, 2014), and additional resistance (Chen et al., 2019b). Based on the linear superposition approach initiated in Zurich, Switzerland (Yen, 2002), we followed the momentum concept, assuming that total resistance can be separated linearly as follows:

$$\tau = \tau' + \tau'', \tag{1}$$

where τ' is riverbed resistance (i.e., grain and form

Table 1 Summary of hydraulic, topographic, and granulometric parameters on the channel-bar interaction regions of the Shashi Reach

Data sets	1	2	3	4	5	6	7	8
Date	August 2003	November 2003	August 2010	November 2010	August 2015	December 2015	March 2018	August 2018
Sets	1165	381	1782	120	1739	403	548	1720
Q (m^3/s)	35000	10000	35000	10000	35000	10000	10000	35000
h_2 (m)	2.970–20.910	0.610–8.590	0.480–16.990	0.080–8.420	0.520–16.940	0.040–9.470	0.040–17.090	0.490–20.090
U (m/s)	0.240–1.670	0.030–0.790	0.030–1.860	0.240–0.700	0.010–1.380	0.010–0.640	0.010–0.730	0.010–1.420
D_{50} (mm)	0.091–0.220	0.097–0.220	0.086–0.260	0.120–0.260	0.094–0.290	0.100–0.290	0.096–0.290	0.096–0.290
J ($\times 10^{-5}$)	7.030–19.160	6.720–10.140	6.100–11.870	3.880–7.380	1.290–14.210	2.280–9.450	1.260–10.480	4.050–15.560
Fr	0.039–0.150	0.011–0.120	0.013–0.310	0.035–0.270	0.005–0.190	0.001–0.140	0.001–0.200	0.004–0.210
Relative width (B/b)	1.210–1.380	1.020–1.350	1.190–1.380	1.030–1.230	1.210–1.380	1.020–1.330	1.020–1.340	1.210–1.380
Relative depth (h_2/h_1)	0.290–0.990	0.120–0.960	0.240–0.890	0.090–0.950	0.210–0.590	0.030–0.460	0.010–0.900	0.190–0.950
Depth/width (h_3/b) ($\times 10^{-4}$)	1–64	1–61	11–85	3–62	42–108	36–79	9–70	8–84

resistance) and τ'' is additional resistance. The effect of friction is quantified through the widely used Manning's roughness coefficient, which is sensitive to the resistance variation with flow and sediment regimes (Ferguson, 2010), thus

$$\frac{n'\sqrt{g}}{R^{1/6}} = \frac{\sqrt{\tau'/\rho}}{U}, \tag{2}$$

$$\frac{n''\sqrt{g}}{R^{1/6}} = \frac{\sqrt{\tau''/\rho}}{U}, \tag{3}$$

where n' and n'' refer to the Manning's roughness coefficients of the riverbed and additional resistance, respectively, ρ refers to the fluid density (kg/m^3), g refers to the gravitational acceleration (m/s^2), and R refers to the hydraulic radius (water depth, m). Hence, to satisfy Eq. (1), we obtain the following:

$$n^2 = n'^2 + n''^2. \tag{4}$$

With respect to riverbed resistance, a widely used empirical model introduced by van Rijn (1984) based on flume and field data can be applied to predict microtopography, including dune height Δ and length λ, and is not, therefore, repeated here. The equivalent roughness height k_s in the van Rijn (1984) model can be computed as follows:

$$k_s = 3D_{90} + 1.1\Delta\left(1 - \mathrm{e}^{-25\Delta/\lambda}\right), \tag{5}$$

where D_{90} is the surface grain diameter of which 90% of the material is finer, and $D_{90} = 1.6D_{50}$ according to local sand-bed sorting (Parker, 1991). Thus, riverbed resistance is derived as follows:

$$n' = \frac{R^{1/6}}{18\lg\left(\frac{12R}{k_s}\right)}. \tag{6}$$

With respect to additional resistance, an extension of the Moreta and Martin-Vide (2010) method, which considers the flow regime and channel geometry, is proposed, as follows:

$$\tau'' = \frac{1}{2}\rho C_{\mathrm{fa}}(\Delta U)^2, \tag{7}$$

$$C_{\mathrm{fa}} = K_{\mathrm{fa}}\left[\left(\frac{B}{b}\right)\left(\frac{h_2}{h_1}\right)^{-\frac{1}{3}}\left(\frac{h_1 - h_2}{b}\right)^{-\frac{1}{3}}\right]^{\alpha}\left(\frac{U}{\Delta U}\right)^{\beta}, \tag{8}$$

where C_{fa} is a non-dimensional friction coefficient acting at the vertical channel-bar interface, ΔU ($= U_1 - U_2$) is the flow velocity difference, U_1 is the average flow velocity in the channel, U_2 is the average flow velocity in the interaction region, and the coefficients K_{fa} and the exponents α and β are used to determine the best fit for C_{fa}. Thus, additional resistance is described as follows:

$$n'' = \frac{(\Delta U)R^{1/6}}{U}\sqrt{\frac{C_{\mathrm{fa}}}{2\mathrm{g}}}. \tag{9}$$

Subsequently, Eqs. (4), (6), and (9) were used to calculate the total, riverbed, and additional resistances, respectively.

3 Results

3.1 Calibration, verification, and evaluation

Based on the detailed hydrometric and bathymetric data, all Manning's roughness coefficients (n_{measured}) were calibrated with water levels and flow velocities at corresponding discharges using HEC-RAS. After calibration through data sets 5–8 (951 low-flow sets and 3459 high-flow sets), pending parameters of 0.035 and 0.016, −0.22 and −0.528, and 1.788 and 2.109 were obtained for K_{fa}, α, and β, respectively (Eq. (8)) for low flows and high flows, with a coefficient of determination of 0.968 and 0.999, respectively. The proposed formula (Eq. (4)) was then verified using data sets 1–4 (501 low-flow sets and 2947 high-flow sets), and the results are shown in Table 2. Our new predictors showed acceptable

Table 2 Performance of different formulae for flow resistance

Investigator	Discharge/(m^3·s^{-1})	Data within different error bands/%					
		±10%	±20%	±30%	DR/%	GSD	RMSE
Peterson and Peterson (1988)	10000	7.12	17.76	28.84	37.91	1.94	0.0167
	35000	19.90	44.34	80.57	20.62	2.34	0.0089
van Rijn (1984)	10000	0.00	0.00	21.35	41.97	1.34	0.0178
	35000	0.05	1.14	39.72	35.43	1.35	0.0145
Present study	10000	36.38	59.87	81.74	17.42	3.69	0.0069
	35000	15.88	42.22	65.40	25.11	2.75	0.0094

Notes: DR, deviation ratio; GSD, geometric standard deviation; RMSE, root mean square error. The evaluation is based on data sets 1−4.

accuracy in channel-bar interaction regions, while the discrepancy ratio (DR) was 17.4% for low flows and 25.1% for high flows (Fig. 2). However, a small difference in the mean prediction error does not necessarily indicate similar predicted flow resistance values between low and high flows. In fact, our proposed formula overestimated flow resistance under low-flow conditions but underestimated it under high-flow conditions.

To further evaluate our formula, two traditional models that are widely applied to the Yangtze River (Huang et al., 2004) were chosen for performance comparison. The first is the van Rijn (1984) model given by Eq. (6), although here, n, is equivalent to n and, therefore, it was not recalculated. The second model is the Peterson-Peterson model (Peterson and Peterson, 1988; Eq. (10)):

$$n = 1.003R^{0.23}J^{0.224}D_{50}^{-0.017}. \quad (10)$$

All of the models were assessed (using data sets 1–4) using statistical indices including the deviation ratio (*DR*), geometric standard deviation (*GSD*), and root-mean-square error (RMSE). Table 2 shows that our proposed model (*DR* = 17.4%) outperformed the van Rijn (*DR* = 42.0%) and Peterson-Peterson (*DR* = 37.9%) models under low-flow conditions. In the case of high-flow conditions, our new model performed better (*DR* = 25.1%) than the van Rijn model (*DR* = 35.4%) but slightly worse than the Peterson-Peterson model (*DR* = 20.6%). Such a difference in model performance between low and high flows may be due to variations in compound hydraulic geometries, which are of great significance in channel-bar-type landscapes.

3.2 Variations in flow resistance with flow conditions and riverbed grain size

Both riverbed resistance and additional resistance changed significantly when the bar was inundated, with a mean increase in riverbed resistance of 22.9% (from 0.020 to 0.025) and a decrease in additional resistance of 43.6% (from 0.039 to 0.021) from low to high flows, respectively (Fig. 3). Riverbed resistance was 0.5- and 1.2-times that of additional resistance at low and high flows, respectively, indicating a shift in the dominant role of total resistance during inundation. This may be attributed to variations in the mean water depth and flow velocity. When the water depth in the channel-bar interaction region is small, the flow velocity here is significantly less than that in the channel, indicating a large flow velocity difference and thus a big additional resistance. In contrast, when the water depth in the channel-bar interaction region is big, the flow velocity difference will be smaller and resulting in a small additional resistance.

Flow resistance showed strong relationships with mean water depths and flow velocities but a weak association with the median diameter of riverbed grains (Fig. 3). Flow resistance increased significantly with increasing water depth, with a mean increase in riverbed resistance of 64.6% and 25.1% at low and high flows, and additional resistance of 90.6% and 115.8%, respectively. A minimum riverbed resistance (0.32 m/s) occurred with an increase above the mean flow velocity, suggesting a strong connection between riverbed resistance and flow regimes. Such a critical flow velocity was also observed by van Rijn (1984) and is likely attributable to form drag in the interaction region, contributing most to riverbed resistance. The transition of flow regimes also has significant impacts on bedforms, including plane beds, ripples, dunes, washed-out dunes, and anti-dunes (Fernandez et al., 2006). However, additional resistance gradually increased with an increase in the mean flow velocity. Furthermore, both riverbed resistance and additional resistance showed a weak relationship with riverbed grain size, indicating that grain resistance contributes little to total resistance in channel-bar interaction regions, which is consistent with sand-bed alluvial channels.

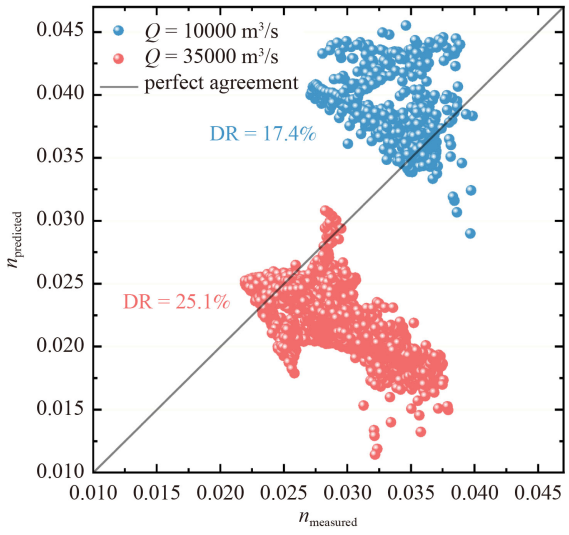

Fig. 2 Comparison of Manning's roughness coefficient (n) for the proposed formula using 501 (2947) sets of data when the discharge rate = 10000 (35000) m³/s. Note that DR is the deviation ratio and Q is discharge.

After the operation of the TGD, there are unavoidable impacts on the Shashi Reach, including its grain size and hydraulic parameters. The median grain size in the channel has increased from 0.019–0.283 mm in 2003 to 0.019–0.315 mm in 2018 (Table 1). Meanwhile, median grain size in the bar has increased from 0.091–0.220 mm in 2003 to 0.096–0.290 mm in 2018 (Table 1). This indicates a potential increase in the riverbed resistance in the channel-bar interaction region in response to the grain coarsening. In the meantime, hungry-water-driven channel erosion causes the amplification of the depth-

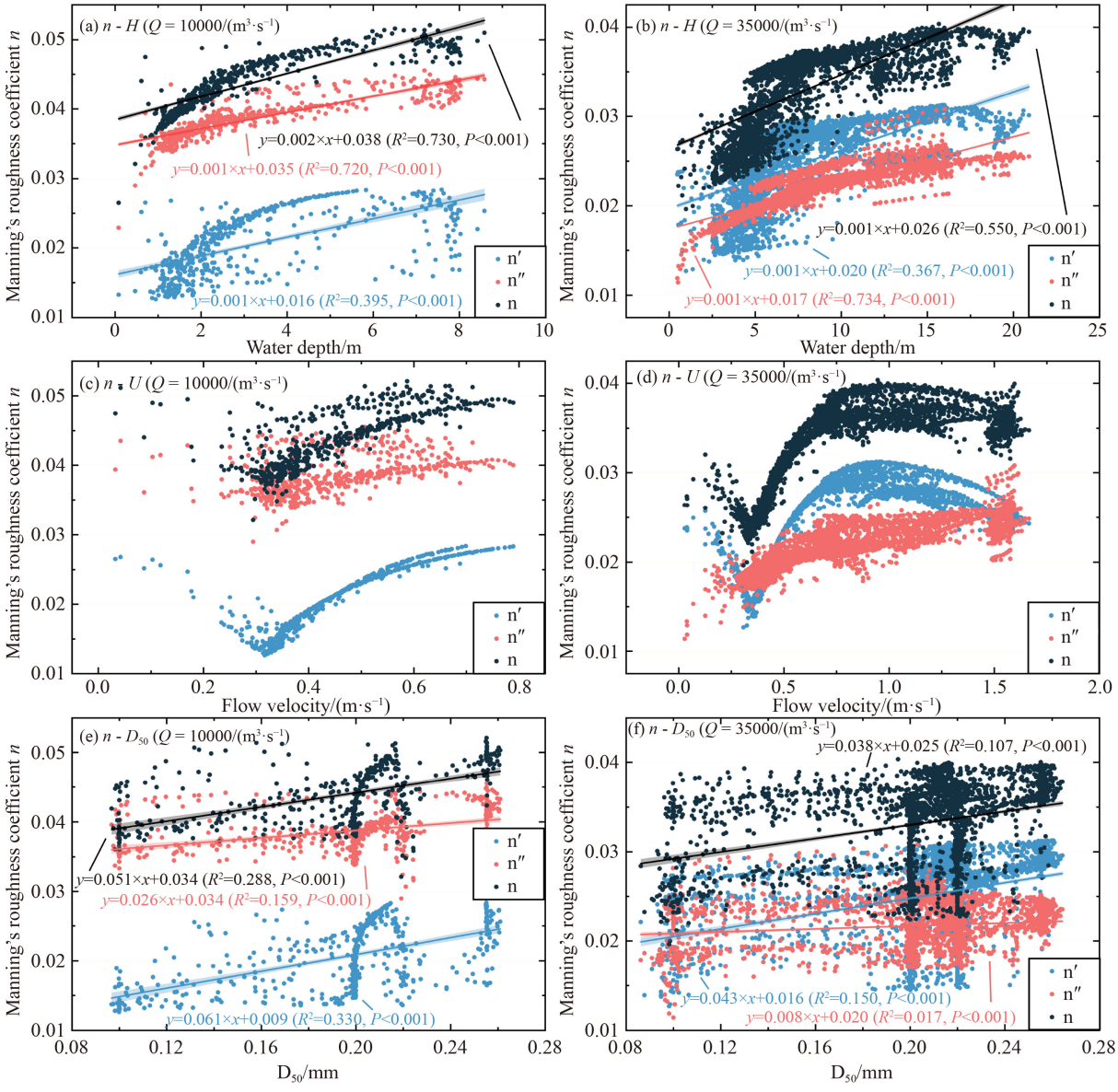

Fig. 3 Variations of flow resistance with water depth (a, b), flow velocity (c, d), and median diameters of riverbed grains (e, f) when the discharge rates = 10000 m^3/s and 35000 m^3/s, respectively. Note that n is total Manning's roughness coefficient, n' is riverbed Manning's roughness coefficient, n'' is additional Manning's roughness coefficient, Q is the discharge, H is the mean water depth, U is the mean flow velocity, and D_{50} is the median diameter of riverbed grains.

width ratio (from 1 to 64 $\times 10^{-4}$ in 2003 to 8–84 $\times 10^{-4}$ in 2018; Table 1), then an enhanced additional resistance in the interaction region may also occur. Therefore, the operation of the TGD may promote the increase of flow resistance in the interaction region of the Shashi Reach.

4 Discussion

4.1 Sensitivity analysis of the impact of hydraulic geometry on flow resistance

To test the performance of our proposed formula for predicting flow resistance in channel-bar interaction regions with variable hydraulic geometry, we selected one set of data from data set 4 to conduct a sensitivity analysis. For these data, h_1 = 6.18 m, h_2 = 3.07 m, B = 1525.01 m, b = 1416.77 m, U_1 = 0.68 m/s, U_2 = 0.37 m/s, and D_{50} = 0.22 mm. The relationships between flow resistance and total width (B), main channel width (b), channel-bar interaction region water depth (h_2), main channel water depth (h_3), mean channel flow velocity (U_1), mean interaction region flow velocity (U_2), and median grain size of the bed material (D_{50}) are shown in Fig. 4.

Riverbed resistance first decreases and then increases as water depth, mean flow velocity, and D_{50} increase in the channel-bar interaction region, which might be

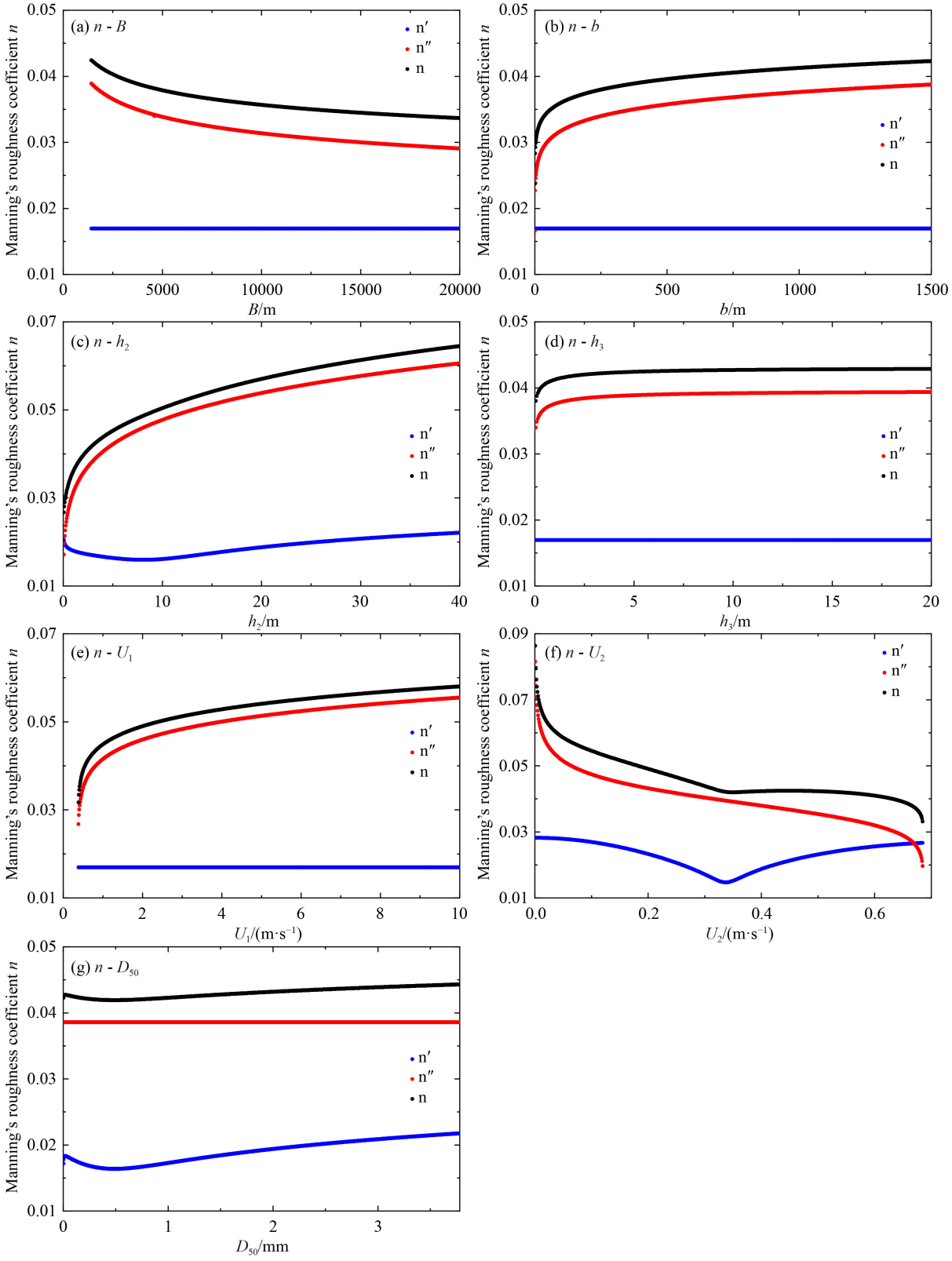

Fig. 4 Variations of flow resistance with (a) B, (b) b, (c) h_2, (d) h_3, (e) U_1, (f) U_2, and (g) D_{50}. The smallest B in (a) is 1416 m because it should at least be wider than the width of the main channel. The smallest U_1 in (e) is 0.37 m/s because it should at least be faster than the flow velocity in the interactive region. Note that n is total Manning's roughness coefficient, n' is riverbed Manning's roughness coefficient, n'' is additional Manning's roughness coefficient, B is the total channel width, b is the main channel width, h_2 is the channel-bar interaction region water depth, h_3 is the main channel water depth, U_1 is the average flow velocity in the channel, U_2 is the average flow velocity in the interaction region, and D_{50} is the median diameter of riverbed grains.

attributed to the bedform variations under different flow regimes (Fig. 4). For example, ripples and dunes may occur or wash out in lower and transitional flow regimes. However, neither changes in the hydraulic parameters of the main channel nor variations in the channel-bar-width ratio affected the riverbed resistance values in the interaction region. Furthermore, the changes in the riverbed Manning's roughness coefficient were small (< 0.02) when the hydraulic parameters varied relative to additional resistance (< 0.05).

Additional resistance is sensitive to all hydraulic geometry parameters except D_{50} (Fig. 4), continuously increasing as B/b and h_2/h_1 decrease, h_3/b increases, or $U/\Delta U$ increases. For each individual parameter, additional resistance shows a positive correlation with b, h_2, h_3, and U_1, and a negative correlation with B and U_2. The relative influence of these factors on additional resistance, in descending order, is $U_2 > h_2 > U_1 > b > B > h_3$. These results indicate that the difference between the channel-bar flow velocities and total water fluxes in channel-bar interface regions are the two dominant factors controlling additional resistance.

4.2 Implications and further research

Previous studies have faced three main limitations when estimating flow resistance in the channel-bar interaction regions of large rivers (Chandra, 2019; Yang et al., 2022). First, calculation models are primarily proposed based on data from laboratories or small rivers (Shiono and Knight, 1991; Chen et al., 2019a). Second, many models are derived under the assumption that the Manning's roughness coefficient in the channel and bar are known and remain constant; however, roughness always has complicated variations as flow and sediment regimes change (Moreta and Martin-Vide, 2010; Chen et al., 2016). Third, earlier models usually assumed that flow resistance in interaction regions is either riverbed resistance or additional resistance, forcing the simplification of complex dynamic changes between the two (Huthoff et al., 2008). Therefore, the resistance equation considering hydraulic geometries and flow regimes that can be applied in large alluvial rivers remains lacking. Importantly, our proposed formulae (Eqs. (4), (6), and (9)) overcome these limitations and, therefore, provide the first model to be successfully applied to the channel-bar-type landscape of a large river, the Shashi Reach of the Yangtze River. Such findings further the understanding of dynamic changes in flow resistance in the channel-bar landscapes of large river systems and have potentially important implications for riverine ecology and flood management.

However, our study remains preliminary with respect to the mechanisms controlling the geomorphological evolution of channel-bar interaction regions, and further work is needed (Church and Ferguson, 2015; Yamaguchi et al., 2019; Zhou et al., 2020; Ferguson et al., 2022). First, large rivers with wider flow regime ranges must be investigated (Fernandez et al., 2006). For instance, a transitional stage with washed-out dunes has been generated for a Froude number of approximately 0.6 in flume experiments (van Rijn, 1984) and 0.2–0.3 in the Missouri River, USA (Shen et al., 1978), yet the mean Froude number in our study was only 0.08. Second, logarithmic or exponential resistance formulas that consider large-scale roughness elements may be alternatives for riverbed resistance calculation where, for example, Eq. (6) cannot be applied to gravel or bedrock channels (Ferguson et al., 2017; Chen et al., 2020). Third, various turbulence parameters in channel-bar interaction regions should be considered when conducting field measurements because of the importance of turbulence information in quantifying velocity distributions (Knight and Shiono, 1990; Chandra, 2019). Fourth, studies concerning erosion and deposition, and sediment and pollutant transport within these interaction regions could be usefully carried out, particularly under various geometry and hydraulic conditions (Paarlberg et al., 2009). Fifth, an extension of our study to vegetated areas should also prove useful (Liu et al., 2020, 2021a, 2021b). Therefore, further application and extension of our proposed flow resistance equations to other global rivers with channel-bar landscapes will yield informative results.

5 Conclusions

We examined the response of riverbed resistance and additional resistance to hydrometric geometry in the channel-bar interaction region of large rivers based on in situ hydro-sediment-bathymetry data for the Shashi Reach of the Yangtze River. We developed a semi-empirical approach for predicting flow resistance that quantifies riverbed resistance and additional resistance separately. Our model outperforms conventional flow resistance models (e.g., the van Rijn model and the Peterson-Peterson model) by integrating dynamic changes into channel geometry, flow, and sediment regimes in the flow resistance calculation.

Overall, our study provides new understanding of a) the intensity of the momentum exchange in the channel-bar interaction regions of large rivers and its greater effects on additional resistance than on riverbed resistance; b) how additional resistance and riverbed resistance decrease and increase, respectively, during bar inundation; and c) the minimum value of riverbed resistance with increases in mean flow velocity. These findings have important implications for assessing fluvial responses to changes in flow and sediment regimes in channel-bar interaction regions and for evaluating associated impacts on hydropower development and

operations, flooding, and aquatic ecosystems. Our insights also underline the need for more field-based turbulence and sediment observations across these interaction regions to better assess the impacts of changing channel-bar landscapes on fluvial systems in the context of climate change and human activity.

References

Arnaud F, Schmitt L, Johnstone K, Rollet A J, Piégay H (2019). Engineering impacts on the Upper Rhine channel and floodplain over two centuries. Geomorphology, 330: 13–27

Bousmar D, Zech Y (1999). Momentum transfer for practical flow computation in compound channels. J Hydraul Eng (NYNY), 125(7): 696–706

Cassells J B C, Lambert M F, Myers R W C (2001). Discharge prediction in straight mobile bed compound channels. Proc Inst Civ Eng Water Marit Eng, 148(3): 177–188

Chandra C S (2019). Analysis of Apparent Shear Stress and Turbulence in Meandering Compound Flows. Dissertation for Master's Degree. Rourkela: National Institute of Technology Rourkela

Chen G, Zhao S, Huai W, Gu S (2019b). General model for stage–discharge prediction in multi-stage compound channels. J Hydraul Res, 57(4): 517–533

Chen X, Hassan M A, An C, Fu X (2020). Rough correlations: meta-analysis of roughness measures in gravel bed rivers. Water Resour Res, 56(8): e2020WR027079

Chen Y, DiBiase R A, McCarroll N, Liu X (2019a). Quantifying flow resistance in mountain streams using computational fluid dynamics modeling over structure‐from‐motion photogrammetry‐derived microtopography. Earth Surf Process Landf, 44(10): 1973–1987

Chen Z, Chen Q, Jiang L (2016). Determination of apparent shear stress and its application in compound channels. Procedia Eng, 154: 459–466

Christodoulou G C (1992). Apparent shear stress in smooth compound channels. Water Resour Manage, 6(3): 235–247

Church M, Ferguson R I (2015). Morphodynamics: rivers beyond steady state. Water Resour Res, 51(4): 1883–1897

Dai Z (2021). Changjiang Riverine and Estuarine Hydro-morphodynamic Processes. New York: Springer

Dai Z, Mei X, Darby S E, Lou Y, Li W (2018). Fluvial sediment transfer in the Changjiang (Yangtze) river-estuary depositional system. J Hydrol (Amst), 566: 719–734

Ferguson R (2010). Time to abandon the Manning equation? Earth Surf Process Landf, 35(15): 1873–1876

Ferguson R (2013). 9.5 Reach-scale flow resistance. In: Shroder J F, ed. Treatise on Geomorphology. San Diego: Academic Press, 50–68

Ferguson R I (2021). Roughness calibration to improve flow predictions in coarse-bed streams. Water Resour Res, 57(6): e2021WR029979

Ferguson R I, Hardy R J, Hodge R A (2019). Flow resistance and hydraulic geometry in bedrock rivers with multiple roughness length scales. Earth Surf Process Landf, 44(12): 2437–2449

Ferguson R I, Lewin J, Hardy R J (2022). Fluvial Processes and Landforms. Geological Society London Memoirs: 58

Ferguson R I, Sharma B P, Hardy R J, Hodge R A, Warburton J (2017). Flow resistance and hydraulic geometry in contrasting reaches of a bedrock channel. Water Resour Res, 53(3): 2278–2293

Fernandez R, Best J, López F (2006). Mean flow, turbulence structure, and bed form superimposition across the ripple‐dune transition. Water Resour Res, 42(5): 2005WR004330

He Z, Sun Z, Li Y, Zhao Q, Hu Y, Chen Z (2022). Response of the gravel–sand transition in the Yangtze River to hydrological and sediment regime changes after upstream damming. Earth Surf Process Landf, 47(2): 383–398

Hooke J M, Yorke L (2011). Channel bar dynamics on multi-decadal timescales in an active meandering river. Earth Surf Process Landf, 36(14): 1910–1928

Huang C, Zhao X, Gong M (2004). Comparisons of flow resistance equations in movable bed. J Sediment Res, 5: 1–7

Huthoff F, Roos P C, Augustijn D C, Hulscher S J (2008). Interacting divided channel method for compound channel flow. J Hydraul Eng (NYNY), 134(8): 1158–1165

Knight D W, Hazlewood C, Lamb R, Samuels P G, Shiono K (2018). Practical Channel Hydraulics: Roughness, Conveyance and Afflux. CRC Press

Knight D W, Shiono K (1990). Turbulence measurements in a shear layer region of a compound channel. J Hydraul Res, 28(2): 175–196

Li D, Lu X X, Chen L, Wasson R J (2019). Downstream geomorphic impact of the Three Gorges Dam: with special reference to the channel bars in the Middle Yangtze River. Earth Surf Process Landf, 44(13): 2660–2670

Li D, Lu X, Overeem I, Walling D E, Syvitski J, Kettner A J, Bookhagen B, Zhou Y, Zhang T (2021). Exceptional increases in fluvial sediment fluxes in a warmer and wetter High Mountain Asia. Science, 374(6567): 599–603

Liu M Y, Huai W X, Chen B (2021a). Predicting the effective diffusivity across the sediment–water interface in rivers. J Clean Prod, 292: 126085

Liu M Y, Huai W X, Yang Z H, Zeng Y H (2020). A genetic programming-based model for drag coefficient of emergent vegetation in open channel flows. Adv Water Resour, 140: 103582

Liu M, Huai W, Ji B (2021b). Characteristics of the flow structures through and around a submerged canopy patch. Phys Fluids, 33(3): 035144

Lou Y, Dai Z, Long C, Dong H, Wei W, Ge Z (2022). Image-based machine learning for monitoring the dynamics of the largest salt marsh in the Yangtze River Delta. J Hydrol (Amst), 608: 127681

Mei X, Dai Z, Darby S E, Gao S, Wang J, Jiang W (2018). Modulation of extreme flood levels by impoundment significantly offset by floodplain loss downstream of the Three Gorges Dam. Geophys Res Lett, 45(7): 3147–3155

Mohanta A, Pradhan A, Mallick M, Patra K C (2021). Assessment of shear stress distribution in meandering compound channels with differential roughness through various artificial intelligence approach. Water Resour Manage, 35(13): 4535–4559

Moreta P J, Martin-Vide J P (2010). Apparent friction coefficient in straight compound channels. J Hydraul Res, 48(2): 169–177

Paarlberg A J, Dohmen‐Janssen C M, Hulscher S J, Termes P (2009).

Modeling river dune evolution using a parameterization of flow separation. J Geophys Res Earth Surf, 114(F01014): 1–17

Parker G (1991). Selective sorting and abrasion of river gravel. II: applications. J Hydraul Eng (NYNY), 117(2): 150–171

Patra K C, Kar S K (2000). Flow interaction of meandering river with floodplains. J Hydraul Eng (NYNY), 126(8): 593–604

Peterson A W, Peterson A E (1988). Mobile boundary flow: an assessment of velocity and sediment discharge relationships. Can J Civ Eng, 15(4): 539–546

Powell D M (2014). Flow resistance in gravel-bed rivers: progress in research. Earth Sci Rev, 136: 301–338

Proust S, Bousmar D, Riviere N, Paquier A, Zech Y (2009). Nonuniform flow in compound channel: a 1-D method for assessing water level and discharge distribution. Water Resour Res, 45(12): 2009WR008202

Shen H W, Harrison A S, Mellema W J (1978). Temperature and Missouri river stages near Omaha. J Hydraul Div, 104(1): 1–20

Shiono K, Knight D W (1991). Turbulent open-channel flows with variable depth across the channel. J Fluid Mech, 222: 617–646

Skalak K J, Benthem A J, Schenk E R, Hupp C R, Galloway J M, Nustad R A, Wiche G J (2013). Large dams and alluvial rivers in the Anthropocene: the impacts of the Garrison and Oahe Dams on the Upper Missouri River. Anthropocene, 2: 51–64

Tellman B, Sullivan J A, Kuhn C, Kettner A J, Doyle C S, Brakenridge G R, Erickson T A, Slayback D A (2021). Satellite imaging reveals increased proportion of population exposed to floods. Nature, 596(7870): 80–86

van Prooijen B C, Battjes J A, Uijttewaal W S (2005). Momentum exchange in straight uniform compound channel flow. J Hydraul Eng (NYNY), 131(3): 175–183

van Rijn L C (1984). Sediment transport, part III: bed forms and alluvial roughness. J Hydraul Eng (NYNY), 110(12): 1733–1754

Wang J, Dai Z, Mei X, Lou Y, Wei W, Ge Z (2018). Immediately downstream effects of Three Gorges Dam on channel sandbars morphodynamics between Yichang–Chenglingji Reach of the Changjiang River, China. J Geogr Sci, 28(5): 629–646

Xia J, Deng S, Lu J, Xu Q, Zong Q, Tan G (2016). Dynamic channel adjustments in the Jingjiang Reach of the Middle Yangtze River. Sci Rep, 6(1): 22802

Yamaguchi S, Giri S, Shimizu Y, Nelson J M (2019). Morphological computation of dune evolution with equilibrium and non-equilibrium sediment-transport models. Water Resour Res, 55(11): 8463–8477

Yang C, Cai X, Wang X, Yan R, Zhang T, Zhang Q, Lu X (2015). Remotely sensed trajectory analysis of channel migration in Lower Jingjiang Reach during the period of 1983–2013. Remote Sens (Basel), 7(12): 16241–16256

Yang X, Sun Z, Deng J, Li D, Li Y (2022). Relationship between the equilibrium morphology of river islands and flow-sediment dynamics based on the theory of minimum energy dissipation. Int J Sediment Res, 37(4): 514–521

Yen B C (2002). Open channel flow resistance. J Hydraul Eng (NYNY), 128(1): 20–39

Zhou M, Xia J, Deng S, Li Z (2022). Two-dimensional modeling of channel evolution under the influence of large-scale river regulation works. Int J Sediment Res, 37(4): 424–434

Zhou Y, Li D, Lu J, Yao S, Yan X, Jin Z, Liu L, Lu X X (2020). Distinguishing the multiple controls on the decreased sediment flux in the Jialing River basin of the Yangtze River, Southwestern China. Catena, 193: 104593